Published in final edited form as:
J Opt Soc Am A Opt Image Sci Vis. 2011 March 1; 28(3): 410–419.

Complete polarization state generator with one variable retarder and its application for fast and sensitive measuring of two-dimensional birefringence distribution

Michael Shribak
Marine Biological Laboratory, 7 MBL St, Woods Hole, MA 02543, USA

Abstract

The complete polarization state generator, which consists of one rotatable polarizer and one variable retarder with quarter-wave plate, is introduced. The orientation angle of its output polarization ellipse equals to half retardance of the variable retarder, and the ellipticity angle corresponds to the polarizer azimuth. The PSG is employed in the quantitative orientation-independent differential polarization microscope, which uses polarized light states with the same ellipticity and different orientation angles. The image processing algorithms with using three or four frames are described.

1. Introduction

A complete polarization state generator (PSG) transforms the incoming light, which is unpolarized or has a constant polarization, into a beam of known polarization state. If the generator can produce a beam of any desired polarization state it is called the complete polarization state generator. When polarized light travels in the inverse direction, the polarization generator extinguishes a beam with the orthogonal polarization. In this case the PSG works as a polarization state analyzer (PSA). The analyzer that can extinguish a beam of any polarization states is called the complete polarization state analyzer. A sequence of the complete PSA and complete PSG can transform any polarization state of the incoming monochromatic light into any polarization state of the coming out light.

The polarization ellipse described by the orientation and ellipticity angles represents polarization state of monochromatic light. In order to control two parameters of the polarization ellipse it is necessary to adjust two independent variables in the polarization state generator at least. Usually the PSG consists of a polarizer and one or several retarders [1–3].

The simplest complete PSG is created by a sequence of a rotated linear polarizer and variable retarder having its fast axis along the X-axis [4]. The amplitude ratio of the polarization components of the output beam in the XY coordinates is equal to the tangent of the polarizer azimuth, and the phase shift between the components is identical to phase difference of the retarder. However the orientation of the polarization ellipse and its ellipticity angle depend trigonometrically on the both polarizer azimuth and retarder phase difference [5]. For example, in order to change the ellipticity only, it would be necessary to

mshribak@mbl.edu .

OCIS Codes: 180.0180, 260.2130, 170.3010, 110.5405, 260.5430, 230.5440.

adjust the polarizer azimuth and the retarder phase difference simultaneously with using trigonometric computations.

There are two basic configurations of arranging optical components in the mentioned complete PSG, when the orientation and ellipticity angles can be controlled independently in the simple way:

(1) The retarder is a quarter-wave plate. The polarizer and quarter-wave plate are installed in a rotatable assembly, where the polarizer can be rotated independently. Orientation of the polarization ellipse corresponds to azimuth of the quarter-wave plate, and ellipticity equals to a difference between polarizer azimuth and quarter-wave plate azimuth. The configuration is known as the Sénarmont compensator [6].

(2) The polarizer is oriented at 45° to the fast axis of the variable retarder, for example a Babinet-Soleil compensator [2]. The polarizer and retarder are placed in a rotatable assembly, where they are rotated simultaneously. In this case the orientation of polarization ellipse corresponds to azimuth of the polarizer, and ellipticity equals to half of phase difference introduced by the retarder [5].

These basic configurations were employed for the quantitative orientation-independent birefringence imaging techniques. The first techniques were reported by and Noguchi et al. [7] and Otani et al. [8]. Noguchi used the first PSG configuration and the left circular analyzer. Otani built his system with modified second PSG configuration and rotatable linear analyzer. Instead of rotating the entire assembly he added a rotated half-wave plate. Pezzaniti and Chipman created a Mueller matrix imaging polarimeter with complete PSG and PSA, which schematic corresponds to the first configuration [9]. We proposed arrangement similar to the first configuration, which consists of rotatable quarter-wave plate and polarized light beamsplitter [10,11]. The device works as a PSG for the beam illuminating a specimen under test and as a PSA for the reflected beam. Using this approach we built two-dimensional birefringence imaging system in the reflected light [12].

Yamaguchi and Hasunuma proposed a dual variable retarder arrangement of the complete PSG without any mechanically moving parts, which consists of two variable retarders oriented at 45° [13,14]. According to this arrangement, Oldenbourg and Mei built the complete PSG with two liquid crystal (LC) cells for using in a quantitative orientation-independent differential polarization microscope called LC-polscope [15,16]. Later we proposed several improved computation algorithms, which increase sensitivity and reduce measurement time of the orientation-independent birefringence imaging [17–20]. Currently, CRI Inc. (Woburn, MA) manufactures systems Oosight and Abrio, which employ the LC-polscope technique and our algorithms (http://www.cri-inc.com). Davis et al. patented a polarimeter with liquid crystals that is based on the dual variable retarder scheme [21]. This arrangement is also used in Mueller matrix imaging polarimeter with Pockels cells by Lara and Dainty [22], Mueller polarimetric imaging system with liquid crystals by Laude-Boulesteix et al. [23]. Mujat and Dogariu employed the dual LC polarization generator for measuring the polarization transfer function [24]. Recently Mujat et al. constructed Mueller matrix microscope, which utilizes dual LC polarization generator and analyzer [25]. Eliminating mechanical rotation increases measurement speed and removes image misalignment caused by rotating optical components. But dual LC systems are not commonly available and they are expensive. The mathematical description of dual variable retarder system is not simple. Orientation and ellipticity of the output polarization ellipse depend trigonometrically on retardance of the both plates simultaneously [20].

De Martino et al. [26] proposed an optimized complete Mueller matrix polarimeter in which the polarization-state generator and analyzer are both composed of a linear polarizer and two

liquid-crystal variable retarders. Garcia-Caurel et al. [27] described a non-imaging spectroscopic complete Mueller matrix polarimeter. The optical setup consists of a polarization states generator and a polarization states analyzer both being identical and using two ferroelectric liquid crystals. Jaulin and Bigue [28] suggest to employ a single non-bistable ferroelectric liquid crystal light modulator for dynamic imaging first three Stokes parameters at high speed.

Here we propose the complete PSG, which consists of one rotatable polarizer and one variable retarder. In our scheme the orientation of polarization ellipse of the emerging beam is determined by retardance of the variable retardation plate only. Therefore a turn of the polarization ellipse does not require mechanical rotation of components. In particularly, the proposed PSG is suitable for a fast differential polarization microscope that employs polarized light states with the same ellipticity and different orientation angles. In principle, a combination of the proposed PSG and PSA can be used as a complete Mueller matrix imaging polarimeter. The PSA can also be employed for imaging Stokes parameter. But we will not consider these applications in the current publication.

2. Description of the Complete Polarization State Generator with One Variable Retarder

A schematic of the proposed complete PSG is shown in Fig.1. It contains in series rotatable polarizer, variable retarder, and quarter-wave plate. Let us choose the slow axis of the variable retarder, which introduces a phase shift α, as X-axis of the Cartesian coordinates. The transmission axis of the polarizer is inclined at an azimuth β from the X-axis. For simplicity of the description we consider angle range $0°\leq\beta\leq90°$. The slow axis of the quarter-wave plate has azimuth −45°. The following matrix-vector product determines the normalized Jones vector of the output beam:

$$\mathbf{E}=\frac{1}{\sqrt{2}}\begin{pmatrix}1 & i\\ i & 1\end{pmatrix}\begin{pmatrix}\exp(-i\alpha/2) & 0\\ 0 & \exp(i\alpha/2)\end{pmatrix}\begin{pmatrix}\cos\beta\\ \sin\beta\end{pmatrix} \tag{1}$$

After multiplication and further trigonometric transformation we obtain:

$$\mathbf{E}=\frac{1}{\sqrt{2}}\begin{pmatrix}\cos\left(\beta+\frac{\alpha}{2}\right)+i\sin\left(\beta-\frac{\alpha}{2}\right)\\ \sin\left(\beta+\frac{\alpha}{2}\right)+i\cos\left(\beta-\frac{\alpha}{2}\right)\end{pmatrix}=\frac{1}{\sqrt{2}}\exp\left(i\arctan\left(\frac{\cos(\beta-\alpha/2)}{\sin(\beta+\alpha\quad 2)}\right)\right)\begin{pmatrix}(1-\sin 2\beta\sin\alpha)^{1/2}\exp\left(-i\arctan\left(\frac{\cos 2\beta}{\sin 2\beta\cos\alpha}\right)\right)\\ (1+\sin 2\beta\sin\alpha)^{1/2}\end{pmatrix} \tag{2}$$

The Jones vector **E** corresponds to polarization ellipse with the next amplitude ratio E_{0x}/E_{0y} and phase difference δ in the initial system of coordinate:

$$\begin{cases}\frac{E_{0x}}{E_{0y}}=\left(\frac{1-\sin 2\beta\sin\alpha}{1+\sin 2\beta\sin\alpha}\right)^{1/2}\\ \delta=\arctan\left(\frac{\cos 2\beta}{\sin 2\beta\cos\alpha}\right)\end{cases} \tag{3}$$

The major axis orientation ψ of the polarization ellipse and its ellipticity angle ε can be found from the known equations [4,5]:

$$\begin{cases} \tan 2\psi = \frac{2E_{0x}E_{0y}}{E_{0x}^2 - E_{0y}^2}\cos\delta \\ \sin 2\varepsilon = \frac{2E_{0x}E_{0y}}{E_{0x}^2 + E_{0y}^2}\sin\delta \end{cases} \quad (4)$$

Using formulae (3) and (4) we can find parameters of the output polarization ellipse:

$$\begin{cases} \varepsilon = 45^\circ - \beta \\ \psi = 45^\circ - \alpha/2, \quad \text{if } \beta \neq 0^\circ \text{ or } 90^\circ \end{cases} \quad (5)$$

In the case β=0° or β=90° the output beam has left or right circular polarization, respectively, and orientation of the polarization ellipse major axis is not defined.

Thus, the proposed polarization generator can produce any polarization state of the output beam:

$$\begin{cases} -45^\circ \le \varepsilon \le 45^\circ, & \text{if } 0^\circ \le \beta \le 90^\circ \\ 0^\circ \le \psi \le 180^\circ, & \text{if } 0^\circ \le \alpha \le 180^\circ \end{cases}$$

The desired ellipticity angle ε can be achieved by rotating the polarizer, and the major axis orientation ψ is determined by phase shift of the variable retarder:

$$\begin{cases} \beta = 45^\circ - \varepsilon \\ \alpha = 90^\circ - 2\psi, \quad \text{if } \varepsilon \pm 45^\circ \end{cases} \quad (6)$$

After substitution angles α and β in equation (2) with angles ε and ψ from (6) we obtain the Jones vector of the output beam expressed by parameters of the polarization ellipse:

$$\mathbf{E} = \begin{pmatrix} \cos\varepsilon \sin\psi - i \sin\varepsilon \cos\psi \\ \cos\varepsilon \cos\psi + i \sin\varepsilon \sin\psi \end{pmatrix} \exp(i\pi/4) \quad (7)$$

The described polarization generator can utilize any variable retarder in order to control the output polarization ellipse orientation. For example, one can employ the Babinet-Soleil compensator [2, 6, 14], the Ehringhaus compensator [6, 29], the Berek compensator [6, 29, 30] or its analogue made of quartz [31], electro-optic or piezo-optical modulator [1, 32], LC variable retarder [32, 33], etc. Instead rotating the polarizer, additional rotatable half-wave plate can be used.

It is possible to employ two proposed PSGs in sequence, where the first PSG creates linearly polarized state with a variable azimuth. It plays a role of rotating polarizer. Example of such device is shown in Fig. 2. The first PSG consists of a LC variable retarder sandwiched between a polymer polarizer and quarter-wave retardation films. The retarder introduces a phase shift γ, where 0°≤γ≤180° for simplicity of explanation. The variable retarder's slow axis is oriented at angle θ to the x-axis. The principal axes of the polarizing and retardation films are parallel and have azimuth of −45° relatively to the slow axis of the first variable retarder.

To obtain parameters of beam passed through the first PSG, we substitute angles γ and 45° for angles α and β respectively, in Eq. (5), and we rotate the polarization ellipse by angle θ:

$$\begin{cases} \varepsilon' = 0° \\ \psi' = 45° + \theta - \gamma/2 \end{cases}$$

Then, in order to find the polarization state of the beam after the second PSG, azimuth Ψ' = 45° + θ − γ /2 is substituted for azimuth β in the first expression of formulae (5):

$$\begin{cases} \varepsilon = \theta - \gamma/2 \\ \psi = 45° - \alpha/2, \quad \text{if } \theta - \gamma/2 \neq \pm 45° \end{cases} \tag{8}$$

In a case when θ = 45°, the slow axis of quarter-wave film of the first PSG is oriented along the X-axis and it is parallel to the slow axis of the second variable retarder LC2. If θ = −45° the slow axes are perpendicular. In these configurations the variable retarder LC2 can also work as a substitute of the first quarter-wave film by adding or subtracting the quarter-wave phase shift. For example, lets consider θ = 45°. The total phase shift α′ of the retarder LC2 could be apportioned as α′=α-90°. Using the equation set (8) the output polarization can be obtained:

$$\begin{cases} \varepsilon = 45° - \gamma/2 \\ \psi' = -\alpha'/2, \quad \text{if } \gamma \neq 0° \text{ or } 180° \end{cases} \tag{9}$$

This modified complete PSG is similar to the dual variable retarder PSG proposed by Yamaguchi and Hasunuma [13, 14]. But adding the quarter-wave retarder with azimuth 45° simplifies the mathematical description of the complete PSG considerably. Ellipticity and azimuth of the output polarization ellipse are directly determined by phase shifts of the first and the second variable retarders, γ and α′, respectively (see Eq. (9)).

3. Polarized Light Microscope with Single Variable Retarder

A. Description of Microscope Setup

The proposed polarization state generator is especially suitable for the quantitative orientation-independent differential polarization microscopy, which employs polarized light with the constant ellipticity and variable orientation angle [16,20]. An example of the microscope, which we call a single liquid crystal polarization microscope (SLC-polscope), is shown in Fig. 3. Here the PSG consists of rotatable linear polarizer P1 and LC cell covered with quarter-wave retardation film QWF. The generated elliptically polarized light is focused on the specimen under investigation S by the condenser. The objective lens creates a magnified image of the specimen on the CCD chip. The imaging beam passes through quarter-wave plate QWP and linear polarizer P2 with the principal axes is oriented at angle 45°. This combination of the quarter waveplate and linear polarizer is often called a circular polarizer (analyzer) since it transmits one circular polarized state and blocks another. But the name is not strictly correct because the transmitted beam has to be circularly polarized, not linearly. The product of the Jones matrices of ideal quarterwave plate and ideal linear polarizer does not correspond to the Jones matrix of the ideal circular polarizer [14]. The true circular polarizer (analyzer) requires the second quarterwave plate in order to transform the emerging linearly polarized light into the circular.

The following Jones matrix-vector product describes polarization transformation of the beam in the optical train of Fig.3:

$$\mathbf{E}(x,y)=\sqrt{\frac{\tau(x,y)}{2}}\begin{pmatrix}1&0\\0&0\end{pmatrix}\begin{pmatrix}1&i\\i&1\end{pmatrix}\times\begin{pmatrix}\cos[\Delta(x,y)/2]-i\cos[2\phi(x,y)]\sin[\Delta(x,y)/2] & -i\sin[2\phi(x,y)]\sin[\Delta(x,y)/2]\\ -i\sin[2\phi(x,y)]\sin[\Delta(x,y)/2] & \cos[\Delta(x,y)/2]+i\cos[2\phi(x,y)]\sin[\Delta(x,y)/2]\end{pmatrix}\times\begin{pmatrix}\cos\varepsilon\sin\psi-i\sin\varepsilon\cos\psi\\ \cos\varepsilon\sin\psi+i\sin\varepsilon\cos\psi\end{pmatrix}\exp(i\pi/4) \tag{10}$$

where Jones vector in the right part represents the polarization state with ellipticity angle ε and the major axis orientation Ψ (see formula (7)); Δ *(x, y)* and θ *(x, y)* are two-dimensional distributions of the specimen's retardance and slow axis orientation respectively; τ*(x,y)* is the distribution of the isotropic specimen transparency; **E** is the Jones vector describing the electrical amplitude distribution in the image.

Carrying out the matrix multiplication in Eq. (10) we find

$$\mathbf{E}(x,y)=\sqrt{\tau(x,y)}\exp(i3\pi/4)\times\begin{matrix}(\cos[\Delta(x,y)/2]\cos(\varepsilon+45^\circ)\exp(-i\psi)+i\sin[\Delta(x,y)/2]\sin(\varepsilon+45^\circ)\exp\{-i[2\phi(x,y)+\psi]\})\\ 0\end{matrix} \tag{11}$$

The intensity distribution in the image *I′(x,y)* obtained by multiplying the Jones vector (11) by the transpose of its complex conjugate is thus

$$I'(x,y)=\frac{1}{2}I(x,y)\tau(x,y)[1-\cos\Delta(x,y)\sin2\varepsilon-\sin\Delta(x,y)\sin2(\phi(x,y)+\psi)\cos2\varepsilon]+\frac{I(x,y)}{\xi(x,y)} \tag{12}$$

Here *I(x,y)* is the distribution of the illumination intensity on the specimen under investigation. We also included the extinction factor ξ*(x,y)* in order to take into account the distribution of the depolarized background illumination. The depolarized light is usually due to imperfect polarizers and optical elements that introduce polarization aberrations [34]. The depolarization component is also caused by multiple scattering in turbid specimens, scattering light on dust particles and scratches in an optical system, nonzero spectral width of illumination, multiple reflections in optical system, and nonflatness of a beam wave front while passing through optical polarization elements.

Reducing the degree of depolarization is very important. For example, the “stray” light with ξ=1000 in the setup with ε=40° contributes the same amount to the total intensity as a particle with 1 nm retardation at wavelength 546 nm. Later, as it is described in section 3.3.D, the depolarized light contribution is subtracted by background correction procedure. However the depolarized “stray” light reduces dynamic range and introduces additional noise, which decreases sensitivity of measuring the birefringent signal.

B. Visual Observation of the Birefringent Specimen with a Sweeping Orientation Angle

The described SLC-polscope can be used for visual observation of birefringence structures in the specimen under investigation by eye, in real-time. For this purpose the polarization

ellipse azimuth Ψ is changed dynamically by the LC variable retarder in order to create a modulated view of the scene (see Eq. (5)):

$$\psi(t) = 45^\circ - \alpha(t)/2. \tag{13}$$

The ellipticity angle ε is remained constant. The specimen is illuminated with a continuum of polarization states, which lie on a latitude line on the Poincare sphere [14]. The longitude, which equals to 2Ψ, is varied continuously. This illumination produces a uniform brightness of non-birefringent surrounding area:

$$I'_{sur}(x,y) = I(x,y)\sin^2(45^\circ - \varepsilon) + \frac{I(x,y)}{\xi(x,y)} \tag{14}$$

Birefringent structures become visible because of their different appearance when modulated against the background. Lets us assume that specimen under investigation is transparent, $\tau(x,y) = 1$. The brightness of a birefringent structure is maximal at $\Psi_{max} = \phi + 45^\circ$:

$$I'_{max}(x,y) = \frac{1}{2}I(x,y)\left[1 - \cos\Delta(x,y)\sin 2\varepsilon + \sin\Delta(x,y)\cos 2\varepsilon\right] + \frac{I(x,y)}{\xi(x,y)} \tag{15}$$

The brightness is minimal at $\Psi_{min} = \phi - 45^\circ$:

$$I'_{min}(x,y) = \frac{1}{2}I(x,y)\left[1 - \cos\Delta(x,y)\sin 2\varepsilon - \sin\Delta(x,y)\cos 2\varepsilon\right] + \frac{I(x,y)}{\xi(x,y)} \tag{16}$$

The image modulation contrast is described by the following formula:

$$k(x,y) = \frac{I'_{max}(x,y) - I'_{min}(x,y)}{I'_{max}(x,y) + I'_{min}(x,y)} = \frac{\sin\Delta(x,y)\cos 2\varepsilon}{1 - \cos\Delta(x,y)\sin 2\varepsilon + \frac{1}{\xi(x,y)}} \tag{17}$$

The contrast depends on the ellipticity angle ε, which is controlled by the polarizer azimuth β (see Eq. (5)). Using a derivative of the function (17) we can find that the maximal contrast occurs when

$$\sin 2\varepsilon_{max} = \frac{1}{1 + 1/\xi}\cos\Delta. \tag{18}$$

The extinction factor of a polarization microscope ξ lies between several hundreds to several thousands [31]. Taking this into account the above expression for ε_{max} can be simplified

$$\sin 2\varepsilon_{max} = (1 - 1/\xi)\cos\Delta \tag{19}$$

In case of large specimen retardance Δ we obtain

$$\varepsilon_{\max}=45^\circ-\Delta/2,\quad \beta_{\max}=\Delta/2,\quad k_{\max}=\frac{\sin^2\Delta}{\sin^2\Delta+1/\xi}. \tag{20}$$

If Δ is small then

$$\varepsilon_{\max}=45^\circ-\left[\left(\frac{\Delta}{2}\right)^2+\left(\frac{90^\circ}{\pi}\right)^2\frac{2}{\xi}\right]^{1/2},\quad \beta_{\max}=\left[\left(\frac{\Delta}{2}\right)^2+\left(\frac{90^\circ}{\pi}\right)^2\frac{2}{\xi}\right]^{1/2},\quad k_{\max}=\frac{\Delta}{\left[\Delta^2+\left(\frac{180^\circ}{\pi}\right)^2\frac{2}{\xi}\right]^{1/2}}. \tag{21}$$

For example, if the specimen retardance Δ=3.6° (or 0.01λ) and ξ=500 then ε_{max}=42.4°, β_{max}=2.6°, and k_{max}=0.70. In this case, according to formulae (14) and (15), brightness of the non-birefringent area is $3.7\times10^{-3}I$ the maximal and minimal brightness of birefringent structure with 0.01 wavelength retardance corresponds to $7.8\times10^{-3}I$ and $2.2\times10^{-3}I$ respectively. The birefringent structure would be visible very well against the background.

A setup for visual observation with one LC variable retarder can employ a simple signal generator of a square wave with frequency 1–10 kHz and sweeping amplitude within a range 2–4 volts. The voltage range of the generator has to provide the LC phase variation α within 360°, which corresponds to changing the ellipse azimuth Ψ by 180°. It is also possible to utilize a “blinking mode”, when the LC retarder generates several polarization states in alternation, which produces a blinking view at the microscope eyepieces. Turning the polarizer can maximize the image contrast. It is convenient to use a cycle frequency about 4 Hz for the best observation. The described system is compatible with integration into other visual microscopy modes such as Zernike phase contrast or Hoffman modulation contrast [35].

C. Mapping Two-Dimensional Birefringence Distribution

1. Polarization States of the Illumination Beam—In order to obtain a quantitative picture of two-dimensional birefringence distribution we capture several images of the specimen under investigation using different polarization states of the illumination beam. Then these polarization images are used to compute 2-dimensional map of retardance magnitude and principal axes orientation. It is convenient to employ polarization states, which have the same ellipticity angle ε and various azimuths of the major axis of the polarization ellipse Ψ. In this case, the raw polarization images could be taken in quick succession by changing phase shift of the LC variable retarder α at constant orientation of the polarizer β (see Eq. (5)).

Figure 4 depicts two groups of used polarization states on the Poincare sphere. The first group, shown on the left, employs 4 polarization states with the same latitude 2ε and different longitudes 2Ψ, 0°, 90°, 180°, and 270°. The corresponding computation algorithm we call the four-frame symmetrical algorithm, as distinct from the previous four-frame algorithm [15,16], which uses 3 polarization states with the polarization ellipse orientations 0°, 45°, 90°, and one circularly polarized state. The second group, illustrated on the right, employs 3 polarization states with the same ellipticity angle and major axis orientations at 0°, 60°, and 120°. The corresponding computation algorithm is called the three-frame symmetrical algorithm.

It is also possible to combine these two algorithms or employ other algorithms using elliptical polarization states with the same latitude on the Poincare sphere in order to reduce

an instrumental error and increase sensitivity. For example, one could easily use two polarization settings with major axis orientations at 0°, 60°, 120° (setting 1) and 30°, 90°, 150° (setting 2). The three-frame algorithm is applied for each set. Then retardance of the specimen under investigation is obtained by averaging the retardances computed in the each set. Orientation angle of the slow axis will be an arithmetic mean of the angle in the first set and the angle rotated by −30° in the second set.

The optimal ellipticity angle ε_{max}, which provides the best contrast, depends on the specimen retardation (see Eq. (20, 21)). If the specimen under investigation has a low retardance the optimal ellipticity angle ε_{max} has to be close to 45°. In this case polarization of the illumination beam is near circular. To measure small retardance values such as those found in living cells, ε_{max} is typically 40° and the polarizer azimuth β_{max} is 5° (see Eq. (6)). If the specimen retardance is large (Δ~90°), then optimal ellipticity ε_{max} equals 0°. Thus the polarizations of used states are linear. In this case the polarizer azimuth β_{max} is 45°.

2. Symmetrical Four-Frame Algorithm—Two columns on the left in Fig.4 illustrate the four-frame processing algorithm, which employs four raw polarization images. Column (a) corresponds to elliptically polarized states of the illumination beam: $\Sigma_1(\varepsilon=\text{const}, \psi_1=0°)$, $\Sigma_2(\varepsilon=\text{const}, \psi_2=45°)$, $\Sigma_3(\varepsilon=\text{const}, \psi_3=90°)$ and $\Sigma_4(\varepsilon=\text{const}, \psi_4=135°)$. These polarization states can be obtained with the following consecutive settings of the polarization state generator (see Eq. (6)): ($\alpha_1=450°$, $\beta=45°-\varepsilon$), ($\alpha_2=360°$, $\beta=45°-\varepsilon$), ($\alpha_3=270°$, $\beta=45°-\varepsilon$), and ($\alpha_4=180°$, $\beta=45°-\varepsilon$).

Intensities of light in the image for each of the polarization states Σ_1, Σ_2, Σ_3 and Σ_4 can be found from Eq. (12):

$$\begin{aligned}
I_1'(x,y) &= \tfrac{1}{2} I(x,y)\,\tau(x,y)\,[1-\cos\Delta(x,y)\cos 2\beta-\sin\Delta(x,y)\sin 2\phi(x,y)\sin 2\beta]+\tfrac{I(x,y)}{\xi(x,y)},\\
I_2'(x,y) &= \tfrac{1}{2} I(x,y)\,\tau(x,y)\,[1-\cos\Delta(x,y)\cos 2\beta-\sin\Delta(x,y)\cos 2\phi(x,y)\sin 2\beta]+\tfrac{I(x,y)}{\xi(x,y)},\\
I_3'(x,y) &= \tfrac{1}{2} I(x,y)\,\tau(x,y)\,[1-\cos\Delta(x,y)\cos 2\beta+\sin\Delta(x,y)\sin 2\phi(x,y)\sin 2\beta]+\tfrac{I(x,y)}{\xi(x,y)},\\
I_4'(x,y) &= \tfrac{1}{2} I(x,y)\,\tau(x,y)\,[1-\cos\Delta(x,y)\cos 2\beta+\sin\Delta(x,y)\cos 2\phi(x,y)\sin 2\beta]+\tfrac{I(x,y)}{\xi(x,y)}.
\end{aligned} \tag{22}$$

The following two term are calculated:

$$\begin{aligned}
A(x,y) &= \frac{I_3'(x,y)-I_1'(x,y)}{I_1'(x,y)+I_3'(x,y)} = \frac{\sin\Delta(x,y)\sin 2\beta}{1-\cos\Delta(x,y)\cos 2\beta+\frac{2}{\xi(x,y)}}\sin 2\phi(x,y),\\
B(x,y) &= \frac{I_4'(x,y)-I_2'(x,y)}{I_4'(x,y)+I_2'(x,y)} = \frac{\sin\Delta(x,y)\sin 2\beta}{1-\cos\Delta(x,y)\cos 2\beta+\frac{2}{\xi(x,y)}}\cos 2\phi(x,y)
\end{aligned} \tag{23}$$

Typically, for a specimen with small retardance about 0.01wavelength (Δ=3.6°), we use the polarizer orientated close to an extinction position with β equals 5°. If ξ=500 then the depolarization contributes about 20% to the denominators in Eq. (23). For imaging specimen with large retardance the polarizer azimuth is 45°. In this case the depolarization contribution is about 0.5%. Therefore the depolarization term can be neglected in further computation, and equations (23) can be simplified:

$$\begin{aligned}
A(x,y) &\ \frac{\sin\Delta(x,y)\sin 2\beta}{1-\cos\Delta(x,y)\cos 2\beta}\sin 2\phi(x,y),\\
B(x,y) &\ \frac{\sin\Delta(x,y)\sin 2\beta}{1-\cos\Delta(x,y)\cos 2\beta}\cos 2\phi(x,y).
\end{aligned} \tag{24}$$

Retardance $\Delta(x,y)$ and slow axis orientation $\phi(x,y)$ can be calculated in the following way:

$$\Delta(x,y) = 2\arctan\left(\frac{\left\{[A(x,y)]^2+[B(x,y)]^2\right\}^{1/2}\tan\beta}{1+\left\{1-[A(x,y)]^2-[B(x,y)]^2\right\}^{1/2}}\right),$$
$$\phi(x,y) = \tfrac{1}{2}\arctan\left[\frac{A(x,y)}{B(x,y)}\right], \quad (25)$$

When the illumination beam is linearly polarized, β=45°, the first formula in Eq. (25) simplifies:

$$\Delta(x,y) = 2\arctan\left(\frac{\left\{[A(x,y)]^2+[B(x,y)]^2\right\}^{1/2}}{1+\left\{1-[A(x,y)]^2-[B(x,y)]^2\right\}^{1/2}}\right).$$

Instead of the considered above four settings of the PSG with α_1=450°, α_2=360°, α_3=270°, and α_4=180°, other sets of four PSG settings with quarter-wavelength step (90°) can be employed as well. But the total required range of phase shift variation α is constant and equals to 270° or 3/4 wavelength. If the major axis orientation of the first polarization ellipse in the set is different from 0°, the retardance computation formula in Eq. (25) can be used without any modification. However the slow axis orientation result has to be corrected by amount of turn of the first polarization ellipse. The correction angle ϕ_{cor} can be found using the following formula:

$$\phi_{cor} = 45^\circ - \alpha_1/2 + 180^\circ m, \quad (26)$$

where *m* is an integer. For example, we can utilize the variable retarder with settings α_1=360°, α_2=270°, α_3=180°, and α_4=90°. In this case the slow axis orientation angle calculated with Eq. (25) has to be corrected by 45°.

3. Symmetrical Three-Frame Algorithm—It is also possible to employ three polarization images. Two columns on the right in Fig.4 represent the corresponding three-frame processing algorithm. Column (a) illustrates the following elliptically polarized states of the illumination beam: $\tilde{\Sigma}_1(\varepsilon=\text{const}, \psi=0^\circ)$, $\tilde{\Sigma}_2(\varepsilon=\text{const}, \psi=60^\circ)$ and $\tilde{\Sigma}_3(\varepsilon=\text{const}, \psi=120^\circ)$. These polarization states can be obtained with the following consecutive settings of the polarization state generator (see Eq. (6)): (α_1=450°, β=45°−ε), (α_2=330°, β=45°−ε), and (α_3=210°, β=45°−ε).

Intensities of light in the image for each of the polarization states can be found from Eq. (12):

$$I_1'(x,y) = \tfrac{1}{2}I(x,y)\tau(x,y)[1-\cos\Delta(x,y)\cos 2\beta - \sin\Delta(x,y)\sin 2\phi(x,y)\sin 2\beta],$$
$$I_2'(x,y) = \tfrac{1}{2}I(x,y)\tau(x,y)[1-\cos\Delta(x,y)\cos 2\beta + \sin\Delta(x,y)\sin(2\phi(x,y)-60^\circ)\sin 2\beta],$$
$$I_3'(x,y) = \tfrac{1}{2}I(x,y)\tau(x,y)[1-\cos\Delta(x,y)\cos 2\beta + \sin\Delta(x,y)\sin(2\phi(x,y)+60^\circ)\sin 2\beta]. \quad (27)$$

Here, for simplicity description, we omit a term associated with the depolarization, as in the previous paragraph.

The captured images $I_1'(x,y)$, $I_2'(x,y)$, and $I_3'(x,y)$ can be combined in the following way:

$$\begin{aligned}
&\left[I_2'(x,y)+I_3'(x,y)\right]-2I_1'(x,y)=\tfrac{3}{2}I(x,y)\,\tau(x,y)\sin\Delta(x,y)\sin 2\phi(x,y)\sin 2\beta,\\
&I_3'(x,y)-I_2'(x,y)=\tfrac{\sqrt{3}}{2}I(x,y)\,\tau(x,y)\sin\Delta(x,y)\cos 2\phi(x,y)\sin 2\beta,\\
&I_1'(x,y)+I_2'(x,y)+I_3'(x,y)=\tfrac{3}{2}I(x,y)\,\tau(x,y)\left[1-\cos\Delta(x,y)\cos 2\beta\right].
\end{aligned} \tag{28}$$

Then we use the next formulae for data processing:

$$\begin{aligned}
A(x,y)&=\frac{\left[I_2'(x,y)+I_3'(x,y)\right]-2I_1'(x,y)}{I_1'(x,y)+I_2'(x,y)+I_3'(x,y)}=\frac{\sin\Delta(x,y)\sin 2\beta}{1-\cos\Delta(x,y)\cos 2\beta}\sin 2\phi(x,y),\\
B(x,y)&=\frac{\sqrt{3}\left[I_3'(x,y)-I_2'(x,y)\right]}{I_1'(x,y)+I_2'(x,y)+I_3'(x,y)}=\frac{\sin\Delta(x,y)\sin 2\beta}{1-\cos\Delta(x,y)\cos 2\beta}\cos 2\phi(x,y).
\end{aligned} \tag{29}$$

From here we calculate retardance and slow axis orientation distributions:

$$\begin{aligned}
\Delta(x,y)&=2\arctan\left(\frac{\left\{\left[A(x,y)\right]^2+\left[B(x,y)\right]^2\right\}^{1/2}\tan\beta}{1+\left\{1-\left[A(x,y)\right]^2-\left[B(x,y)\right]^2\right\}^{1/2}}\right),\\
\phi(x,y)&=\tfrac{1}{2}\arctan\left[\frac{A(x,y)}{B(x,y)}\right],
\end{aligned} \tag{30}$$

As an alternative of the considered three settings of the PSG with α_1=450°, α_2=330°, and α_3=210°, other sets of three PSG settings with the third-wavelength step (120°) can be employed as well. The total required range of phase shift variation α is constant and equals to 240° or 2/3 wavelength. If the major axis orientation of the first polarization ellipse in the set is different from 0°, the slow axis orientation result has to be corrected according to the formula (26).

4. Correction of Background Retardance—When measuring a specimen with small retardance, it is important to minimize errors that are due to background retardance. Lenses, optical flats and other optical components, that are located between the polarizer and the analyzer of the microscope, contribute to the background retardance [34]. The spatially varying background retardance leads to systematic error in the measurement of specimen retardances.

For correction of the background retardance it is possible to employ special procedure, which mathematical description we published early [20]. The procedure is based on specimen images, which are recorded with no birefringent particles in the optical path. In order to record the background set of images the object is moved out of the camera view field by use of the x-y translator of the microscope. If empty area around the object is not available one could utilize a defocused picture of the object as the background. The background images are captured at the same polarization generator settings as for the object itself. Using these images we compute terms $\boldsymbol{A_{bg}}(x,y)$ and $\boldsymbol{B_{bg}}(x,y)$ according to formulae (23) or (29). Then the differences between the terms $\boldsymbol{A}(x,y)$-$\boldsymbol{A_{bg}}(x,y)$ and $\boldsymbol{B}(x,y)$-$\boldsymbol{B_{bg}}(x,y)$ are used in modified formulas (25) and (30) for determining retardance and slow axis orientation:

$$\begin{aligned}
\Delta(x,y)&=2\arctan\left(\frac{\left\{\left[A(x,y)-A_{bg}(x,y)\right]^2+\left[B(x,y)-B_{bg}(x,y)\right]^2\right\}^{1/2}\tan\beta}{1+\left\{1-\left[A(x,y)-A_{bg}(x,y)\right]^2-\left[B(x,y)-B_{bg}(x,y)\right]^2\right\}^{1/2}}\right),\\
\phi(x,y)&=\tfrac{1}{2}\arctan\left(\frac{A(x,y)-A_{bg}(x,y)}{B(x,y)-B_{bg}(x,y)}\right),
\end{aligned} \tag{31}$$

In addition to correcting background retardance of the specimen under investigation this procedure also accounts for slight miscalibration of polarization states of the illumination beam: Σ_1, Σ_2, Σ_3, Σ_4 (in case of the four-frame algorithm), and $\tilde{\Sigma}_1$, $\tilde{\Sigma}_2$, $\tilde{\Sigma}_3$ (in case of the three-frame algorithm).

Typically, the background retardance does not change considerably over a time period of many minutes. Therefore the intermediate results $\boldsymbol{A_{bg}}(x,y)$ and $\boldsymbol{B_{bg}}(x,y)$ can be employed repeatedly to correct, e.g., a time series of images measuring the subtle changes in birefringence in a live specimen.

It is possible that intensity of the illumination would fluctuate during the time series image acquisition. We observed such fluctuations using high power mercury arc lamps. Also retardance of the LC retarder could slightly vary because of a temperature change. These reasons of an error in the measured specimen retardance distribution cannot be corrected with the described background correction procedure. But this small error retardance would be uniform across the image. Therefore if there is an image area with known retardance we can use it for additional correction. For example, the obtained image shows some retardance Δ_{cor} and slow axis orientation ϕ_{cor} in an image point where the retardance is expected to be zero. This allows us to compute the correction terms $\boldsymbol{A_{cor}}$ and $\boldsymbol{B_{cor}}$ using equations (24) or (29):

$$\begin{aligned} A_{cor} &= \frac{\sin\Delta_{cor}\sin 2\beta}{1-\cos\Delta_{cor}\cos 2\beta}\sin 2\phi_{cor}, \\ B_{cor} &= \frac{\sin\Delta_{cor}\sin 2\beta}{1-\cos\Delta_{cor}\cos 2\beta}\sin 2\phi_{cor}. \end{aligned} \tag{32}$$

Then the obtained terms are applied for calculating the corrected retardance and slow axis orientation for the entire image:

$$\begin{aligned} \Delta(x,y) &= 2\arctan\left(\frac{\left\{\left[A(x,y)-A_{bg}(x,y)-A_{cor}\right]^2+\left[B(x,y)-B_{bg}(x,y)-B_{cor}\right]^2\right\}^{1/2}\tan\beta}{1+\left\{1-\left[A(x,y)-A_{bg}(x,y)-A_{cor}\right]^2-\left[B(x,y)-B_{bg}(x,y)-B_{cor}\right]^2\right\}^{1/2}}\right), \\ \phi(x,y) &= \frac{1}{2}\arctan\left(\frac{A(x,y)-A_{bg}(x,y)-A_{cor}}{B(x,y)-B_{bg}(x,y)-B_{cor}}\right). \end{aligned} \tag{33}$$

The formulas (33) allow to receive retardation images, which are corrected on the background retardance, illumination intensity fluctuations and LC retardance variations.

5. Experimental Verification—To experimentally analyze the data processing algorithms we employed microscope Olympus BX-61 (Olympus America Inc., Center Valley, PA) equipped with a liquid-crystal variable retarder and other polarization components according to the scheme shown in the Fig. 3. We tested LC variable retarders made by ARCoptix (Switzerland) and Boulder Vision Optik (Boulder, CO). The Bolder Vision retarder had considerably better quality. Also its price was about a half price of the ARCoptix variable retarder. We used a 40×/0.75P UPlanFL objective lens (Olympus); a narrow-bandpass interference filter (546 nm, 10-nm FWHM; Chroma Technology, Rockingham, VT); and monochromatic CCD camera Infinity 3-1M (Lumenera, Canada). We accomplished image acquisition and analysis using MATLAB (the MathWorks Inc., Natick, MA), which was enhanced by custom software functions.

Initially we set up azimuth β the polarizer P1 at 0°. In this case the illumination beam became the circularly polarized independently on the phase shift α introduced by the LC cell. Then, using an empty area in the specimen under investigation, we achieve the minimal image intensity by subtle turns of the components of the circular analyzer, quarter-wave

plate QWP and linear polarizer P2. This adjustment of the circular analyzer compensates the specimen background retardance. After that we capture an image of the specimen with empty area in the center and a picture with the illumination OFF. Next we turn the polarizer P1 by angle β, typically 5°, and take new image of the specimen. Using the obtained picture the extinction factor ξ can be calculated in the following way:

$$\xi=\frac{1}{\sin^2\beta}\frac{I_\beta - I_0}{I_0 - I_{dark}}, \tag{34}$$

where I_β, I_0, and I_{dark} are intensities are intensities in the empty area when the polarizer is oriented at angles β, 0°, and without illumination, correspondently. This formula could be derived from equation (22) at Δ=0°.

Afterward we recorded two sets of specimen and background images at polarization states (Σ_1, Σ_2, Σ_3, Σ_4) and ($\tilde{\Sigma}_1$, $\tilde{\Sigma}_2$, $\tilde{\Sigma}_3$) as described in Subsections 3.3.B and 3.3.C. Subsequently the raw polarization images were processed with the four-frame and three-frames algorithms with background correction as explained in Subsections 3.3.D. Then we took retardance image of the same specimen under investigation using a regular LC-polscope with two LC variable retarders [20].

Figure 5 shows an example of retardance image of Diatom test plate [36], which was computed with using three-frames algorithm. Three raw polarization images of the specimen $\boldsymbol{I}_1$, $\boldsymbol{I}_2$, $\boldsymbol{I}_3$ are shown in the left, and three background images $\boldsymbol{I}_{bg1}$, $\boldsymbol{I}_{bg2}$, $\boldsymbol{I}_{bg3}$ are depicted in the right. The extinction factor ξ was 1100, and polarizer angle β was 5°. Brightness of the 8-bit grayscale image is linearly proportional to the computed retardation Δ, where white corresponds to the maximal retardance Δ_{max}=5nm and black corresponds to zero retardance. However areas with zero retardance are not completely black because of noise. Retardance images obtained with proposed SLC-polscope and regular LC-polscope demonstrate very similar noise level. The noise floor corresponds the smallest birefringent signal that can be measured. In particularly the SLC-polscope yielded the noise floor of 0.047 nm with three-frame algorithm and 0.05 nm with four-frame algorithm. The regular LC-polscope had noise of 0.049 nm.

4. Conclusion

Here we are proposing new complete polarization state generator, which consists of one rotatable polarizer and one fixed variable retarder. Ellipticity of the output beam is determined by orientation of the polarizer while the major axis azimuth of the beam is defined by optical path difference of the waveplate.

The polarization state generator was employed in a polarized light microscope with single liquid crystal variable retarder (SLC-polscope) for fast and sensitive mapping two-dimensional birefringence distribution. We developed new processing algorithms for application with new SLC-polscope.

The proposed SLC-polscope provides practically the same results as existing LC-polscope with dual variable retarder, which is available on the market. But our approach has the following advantages:

- SLC-polscope allows more easy implement retardation mapping algorithms using polarization states with the same ellipticity and realize blinking mode for visual studying birefringent specimens.

- SLC-polscope could have considerably faster response time. It employs rising voltage during the image acquisition. Polscope with dual LC variable retarder uses both rising and declining voltages. The electric field applies an external “torque” to each molecule, but, when the field is reduced, interactions between LC molecules provide the dominant restoring forces. These interactive forces are much weaker than the torque caused by an external electrical field. Therefore activation time could be 40 times shorter then relaxation time.
- SLC-polscope would be more easy integrate with other microscope modalities because it has smaller thickness (~2.5mm, which is about a half of the two LC scheme).
- Dual LC variable retarders themselves are not available on the market. Their manufacturing is difficult and expensive. Single LC variable retarders are freely available and cheap.
- LC variable retarders are sensitive to temperature variation, wavelength range, and incidence angle. These retarders introduce depolarization and wavefront aberrations. Using one such component instead of two would improve the image quality.
- SLC-polscope could employ more bulky and expensive one electro-optical variable retarder instead of a liquid crystal retarder. That would allow us to increase response time from tens milliseconds to a nanosecond, work in UV and IR spectral regions, etc.

Acknowledgments

The author is grateful to Dr. Shinya Inoué of the Marine Biological Laboratory (MBL), Woods Hole, MA for helpful discussion and encouragement of this research. The author thanks Amitabh Verma and Richard Langill of the MBL for software and hardware developments respectively; Yuri Shabeta (Minsk, Belarus) for design and fabricating mechanical components. This publication was made possible by Grant Number RO1-EB005710 from the National Institute of Biomedical Imaging and Bioengineering, National Institutes of Health. Its contents are solely the responsibility of the author and do not necessarily represent the official views of the National Institute of Biomedical Imaging and Bioengineering or the National Institutes of Health.

References

1. Hauge PS. Recent Development In Instrumentation In Ellipsometry. Surface Sci. 1980; 96:108–140.
2. Goldstein, D. Polarized Light. 2nd ed.. Marcel Dekker; New York: 2003.
3. Chipman, RA. Polarimetry. In: Bass, M.; Mahajan, VN., editors. Handbook of Optics, Third Edition, Volume I: Geometrical and Physical Optics, Polarized Light, Components and Instruments. McGraw-Hill; 2009. p. 15.1-15.46.
4. Collett, E. Polarized Light in Fiber Optics. PolaWave; Lincroft, New Jersey: 2003.
5. Shribak, M. Polarization. In: Yoshizawa, T., editor. Handbook of Optical Metrology: Principles and Applications. CRC Press; Boca Raton, Florida: 2009. p. 339-350.
6. Hartshorne, NH.; Stuart, A. Crystals and the Polarizing Microscope. 4th ed.. Edward Arnold; London, United Kingdom: 1970.
7. Noguchi M, Ishikawa T, Ohno M, Tachihara S. Measurement of 2D birefringence distribution. International Symposium on Optical Fabrication, Testing, and Surface Evaluation, Proc. SPIE. 1992; 1720:367–378.
8. Otani Y, Shimada T, Yoshizawa T, Umeda N. Two- dimensional birefringence measurement using the phase shifting technique. Opt. Eng. 1994; 33:1604–1609.
9. Pezzaniti JL, Chipman RA. Mueller matrix imaging polarimeter. Opt. Eng. 1995; 34:1558–1568.
10. Shribak M. Device for measuring birefringence of reflecting optical data carrier. March 17.1986 Patent of the USSR 1414097.

11. Shribak M. A compensation method for measuring birefringence. Sov. J. Opt. Technol. 1993; 60:546–549.
12. Shribak M, Otani Y, Yoshizawa T. Autocollimation polarimeter for measuring two-dimensional distribution of birefringence. Optics & Spectroscopy. 2000; 89:155–159.
13. Yamaguchi T, Hasunuma H. A quick response recording ellipsometer. Science of Light. 1967; 16:64–71.
14. Azzam, RMA.; Bashara, NM. Ellipsometry and Polarized Light. Elsevier Science; Amsterdam, Netherlands: 1987.
15. Oldenbourg R, Mei G. Polarized light microscopy. May 12.1994 US Patent 5521705.
16. Mei G, Oldenbourg R. Fast imaging polarimetry with precision universal compensator. Polarization Analysis and Measurement II, Pros. SPIE. 1994; 2265:29–39.
17. Shribak M, Oldenbourg R. Retardance measurement system and method. July 8.2003 US Patent 7202950.
18. Shribak M, Oldenbourg R. Retardance measurement system and method. July 8.2003 US Patent 7239388.
19. Shribak M, Oldenbourg R. Retardance measurement system and method. July 8.2003 US Patent 7372567.
20. Shribak M, Oldenbourg R. Techniques for fast and sensitive measurements of two-dimensional birefringence distributions. Applied Optics. 2003; 42:3009–3017. [PubMed: 12790452]
21. Davis SR, Uberna RJ, Herke RA. Retardance sweep polarimeter and method. August 20.2002 US Patent 6744509.
22. Lara D, Dainty C. Double-pass axially resolved confocal Mueller matrix imaging polarimetry. Optics Letters. 2005; 30:2879–2881. [PubMed: 16279456]
23. Laude-Boulesteix B, De Martino A, Drevillon B, Schwartz L. Mueller polarimetric imaging system with liquid crystals. Applied Optics. 2004; 43:2824–2832. [PubMed: 15143805]
24. Mujat M, Dogariu A. Real-time measurement of the polarization transfer function. Applied Optics. 2001; 40:34–44. [PubMed: 18356971]
25. Mujat, M.; Iftimia, N.; Ferguson, RD.; Hammer, DX. Biomedical Optics (BIOMED)/ Digital Holography and Three-Dimensional Imaging (DH), CDROM. Optical Society of America; 2010. Mueller Matrix Microscopy. paper BSuD60
26. De Martino A, Kim Y-K, Garcia-Caurel E, Laude B, Drévillon B. Optimized Mueller polarimeter with liquid crystals. Optics Letters. 2003; 28:616–618. [PubMed: 12703918]
27. Garcia-Caurel E, De Martino A, Drevillon B. Spectroscopic Mueller polarimeter based on liquid crystal devices. Thin Solid Films. 2004; 455–456:120–123.
28. Jaulin A, Bigue L. High speed partial Stokes imaging using a ferroelectric liquid crystal modulator. Journal of the European Optical Society - Rapid Publications. 2008; 3:08019.
29. Holmes DA. Wave Optics Theory of Rotary Compensators. J. Opt. Soc. Am. 1964; 54:1340–1347.
30. Rinne, F.; Berek, M. Anleitung zu Optischen Untersuclhungen mit dem Polarizationsmikroskop. Schweizerbart'sche Verlagsbuchhandlung; Stuttgart, Germany: 1953.
31. Shribak M. Use of gyrotropic birefringent plate as quarter-wave plate. Sov. J. Opt. Technol. 1986; 53:443–446.
32. Yariv, A.; A.; Yeh, P. Optical Waves in Crystals: Propagation and Control of Laser Radiation. John Wiley & Sons; New York: 1984.
33. Scharf, T. Polarized Light in Liquid crystals and Polymers. John Wiley & Sons; Hoboken, New Jersey: 2007.
34. Shribak M, Inoué S, Oldenbourg R. Polarization aberrations caused by differential transmission and phase shift in high NA lenses: theory, measurement and rectification. Optical Engineering. 2002; 41:943–954.
35. Oldenbourg, R.; Shribak, M. Microscopes. In: Bass, M.; Mahajan, VN., editors. Handbook of Optics, Third Edition, Volume I: Geometrical and Physical Optics, Polarized Light, Components and Instruments. McGraw-Hill; 2009. p. 28.1-28.62.
36. Salmon ED, Tran P. High resolution video-enhanced differential-interference contrast (VE-DIC) light microscopy. Meth. Cell Biol. 1998; 56:153–185.

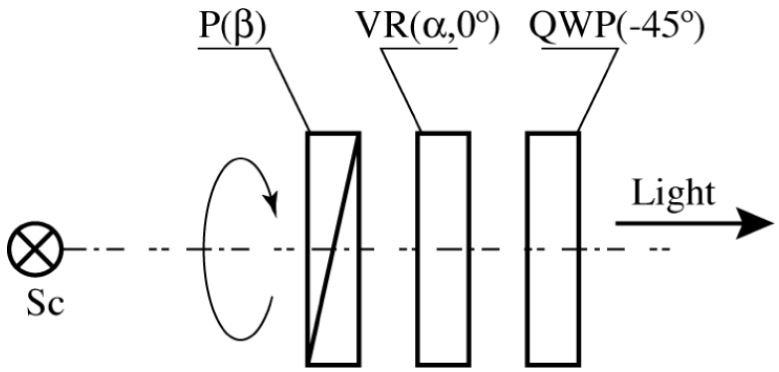

Fig.1.

Schematic of complete polarization state generator with rotatable polarizer and one variable retarder. Here **Sc** is a monochromatic light source, **P** is linear polarizer, **VR** is variable retarder, and **QWP** is quarter-wave plate. X-axis of the Cartesian coordinates corresponds to the slow axis of the variable retarder. Angle β is orientation of transmission axis of the polarizer. The variable retarder introduces a phase shift α.

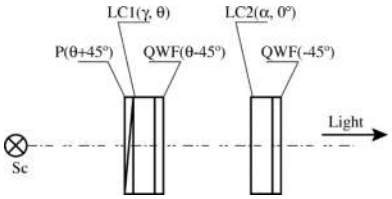

Fig.2.

Schematic of complete polarization state generator with fixed polarizer and two liquid crystal variable retarders. Here **Sc** is a monochromatic light source, **P** is fixed linear polarizer, **LC1** and **LC2** are liquid crystal variable retarders, and **QWF**s are achromatic quarter-wave retardation films. X-axis of the Cartesian coordinates corresponds to the slow axis of the second LC variable retarder. Angle θ is orientation of slow axis of the first LC variable retarder. The variable retarders **LC1** and **LC2** introduce phase shifts γ and α, respectively.

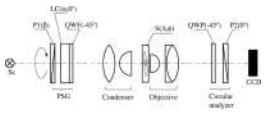

Fig.3.

Example of the quantitative orientation-independent differential polarization microscope (SLC-polscope) with proposed complete polarization state generator. Here **Sc** is a monochromatic light source; **PSG** is polarization state generator consisting of rotatable linear polarizer **P1** and liquid crystal cell **LC** covered with achromatic quarter-wave retardation film **QWF**; **S** is the specimen under investigation; achromatic quarter-wave plate **QWP** and second linear polarizer **P2**, which together construct a left-handed circular analyzer; **CCD** is an imaging detector (CCD camera). Δ (*x, y*) and ϕ (*x, y*) are two-dimensional distributions of the specimen's retardance and slow axis orientation.

Fig.4.

Polarization states of illumination beam on the Poincare sphere. The left column in the left group depicts four elliptical polarization states Σ_1, Σ_2, Σ_3 and Σ_4 used with the four-frame algorithm for imaging specimen with low retardance. They are shown in triangles on the Poincare sphere. The right column in this group illustrates four linear polarization states $\tilde{\Sigma}_1'$, $\tilde{\Sigma}_2'$, $\tilde{\Sigma}_3'$ and $\tilde{\Sigma}_4'$ used for imaging specimen with high retardance. They are shown in diamonds on the sphere. The left column in the right group represents three elliptical polarization states $\tilde{\Sigma}_1$, $\tilde{\Sigma}_2$, and $\tilde{\Sigma}_3$ used with the three-frame algorithm for imaging specimen with low retardance. They are shown in shaded square box on the Poincare sphere. The right column in this group illustrates 3 linear polarization states $\tilde{\Sigma}_1'$, $\tilde{\Sigma}_2'$, and $\tilde{\Sigma}_3'$, used for imaging specimen with high retardance. They are shown in shaded circle on the sphere.

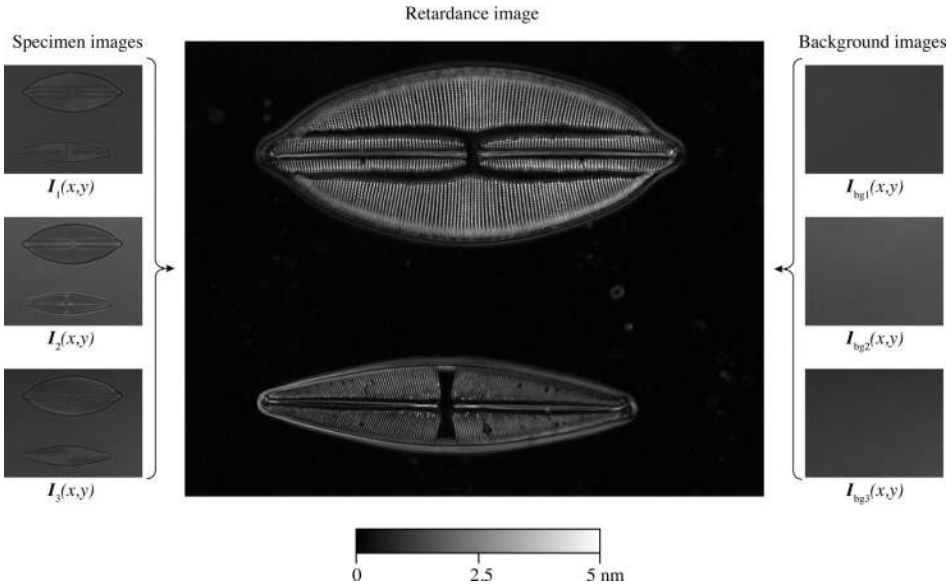

Fig.5.

Images of Diatom test plate obtained with SLC-polscope: three raw specimen and three background intensity images captured in a time sequence by the monochromatic camera (on the left and the right, respectively); computed with the symmetrical three-frame algorithm retardance image after background correction (in the center). Image brightness is linearly proportional to retardance where white corresponds to the maximal retardance Δ_{max}=5nm and black corresponds to zero retardance.